



CHALMERS
UNIVERSITY OF TECHNOLOGY

Understanding the impact of steam pretreatment severity on cellulose ultrastructure, recalcitrance, and hydrolyzability of Norway spruce

Downloaded from: <https://research.chalmers.se>, 2026-04-04 17:42 UTC

Citation for the original published paper (version of record):

Caputo, F., Al-Rudainy, B., Naidjonoka, P. et al (2022). Understanding the impact of steam pretreatment severity on cellulose ultrastructure, recalcitrance, and hydrolyzability of Norway spruce. *Biomass Conversion and Biorefinery*, In Press. <http://dx.doi.org/10.1007/s13399-022-03405-0>

N.B. When citing this work, cite the original published paper.



Understanding the impact of steam pretreatment severity on cellulose ultrastructure, recalcitrance, and hydrolyzability of Norway spruce

Fabio Caputo¹ · Basel Al-Rudainy² · Polina Naidjonoka^{3,4} · Ola Wallberg² · Lisbeth Olsson^{1,3} · Vera Novy^{1,3}

Received: 1 July 2022 / Revised: 26 September 2022 / Accepted: 11 October 2022
© The Author(s) 2022

Abstract

The efficient use of softwood in biorefineries requires harsh pretreatment conditions to overcome biomass recalcitrance. Following harsh pretreatments, the hemicellulose is solubilized. Here, we studied the material characteristics of Norway spruce following steam pretreatment at six different severities, relating chemical and structural information to the enzymatic hydrolyzability. Steam pretreatment conditions were defined by two different temperatures (180 °C and 210 °C), with and without the addition of various acids (CH₃COOH, H₃PO₄, H₂SO₄, SO₂). Structural knowledge of the streams is a cornerstone for developing an efficient saccharification process.

This study combines advanced structural characterizations to gain fundamental understanding of the influence of severity of pretreatment on spruce. Structural knowledge is a cornerstone in developing an effective saccharification process by modulating pretreatment conditions and enzymes employed.

Overall structural properties were assessed by scanning electron microscopy. The effect of stream pretreatment severity on lignin and lignin-carbohydrate bonds was investigated by two-dimensional heteronuclear single quantum correlation nuclear magnetic resonance. Finally, cellulose ultrastructure was studied by applying small/wide-angle X-ray scattering. The structural characteristics of the six pretreated softwood substrates were related to the enzymatic hydrolyzability.

With increasing pretreatment severity, surface defibrillation, and lignin depolymerization were observed. Further, lignin-carbohydrate complexes signals were detected. Cellulose analysis revealed the rearrangement of microfibrils leading to the formation of larger microfibril aggregates. This microfibril rearrangement likely contributed to the observed increase in enzymatic hydrolysis yields as better enzyme accessibility resulted.

Keywords Cellulose accessibility · SEM · SAXS/WAXS · 2D HSQC-NMR · Lignin carbohydrate bonds · Softwood

1 Introduction

Pollution, climate change, waste accumulation, and depletion of natural resources have increased at an alarming rate as a result of human activity [1]. Biorefineries, which produce biofuels and chemicals from lignocellulosic biomass, may address some of these challenges. Biorefinery processes might consist of five main unit operations: pretreatment, enzymatic hydrolysis, fermentation — combined or not with hydrolysis — product recovery, and wastewater purification [2]. All unit operations have to be adapted to the desired product and the available feedstock. In order to adapt the process to the feedstock and design the process steps, it is important to add structural knowledge on the different lignocellulosic biomasses. In Sweden, almost 70% of the land is forest, and the 83% of it is coniferous composed by 40% spruce, making spruce a viable feedstock for biorefineries.

✉ Lisbeth Olsson
lisbeth.olsson@chalmers.se

¹ Division of Industrial Biotechnology, Department of Biology and Biological Engineering, Chalmers University of Technology, Kemivägen 10, 412 96 Gothenburg, Sweden

² Department of Chemical Engineering, Lund University, Naturvetarvägen 14, 22100 Lund, Sweden

³ Wallenberg Wood Science Center, Chalmers University of Technology, Kemigården 4, 412 96 Gothenburg, Sweden

⁴ Division of Materials Physics, Department of Physics, Chalmers University of Technology, Kemigården 1, 412 96 Gothenburg, Sweden

Spruce is composed of cellulose (45–47% w/w DM [3]), hemicelluloses (up to 15% w/w dry mass (DM) arabinoglucuronoxylan and up to 30% w/w DM galactoglucomannan [4]), and lignin (27–28% w/w DM [3]).

Low enzymatic hydrolysis efficiencies of softwood represent one of the main hurdles to industrial-scale biorefinery applications. Enzymatic hydrolysis of lignocelluloses is affected by substrate- and enzyme-related parameters. Enzyme-related parameters have been studied extensively, resulting in a relatively good understanding [5]. Apart from direct substrate features, such as the S/G ratio of lignin [6], substrate-related parameters are mainly associated with the accessibility of cellulose to cellulytic enzymes [5]. Accessibility can be restricted by the hemicellulose and lignin matrix, in which cellulose fibers are embedded [7]. Additionally, hemicellulose and lignin can be covalently linked to form lignin-carbohydrate complexes (LCCs), further increasing substrate recalcitrance [8–10]. Another key role is played by cellulose ultrastructure (i.e., degree of organization on micro-, macro-, and fiber level) [5, 11–13]. A direct and quantitative link between a lower degree of organization (i.e., higher accessibility) and increased hydrolyzability has been established recently [14]. However, it is necessary to obtain a detailed understanding of substrate ultrastructure and how it affects the enzymatic hydrolyzability in non-model substrates that contain not only cellulose, but also hemicellulose and/or lignin [14].

Collectively, these substrate-related limitations require a pretreatment step to obtain sugar release by enzymatic hydrolysis. Steam pretreatment (STEX) offers a mature and flexible technology in this respect [15, 16], but necessitates the addition of acids to compensate for the low amount of organic acids in softwood [16–18]. Because spruce has acetyl groups only on the galactoglucomannan [4] — 1 acetyl group only every 3/4 hexose units [19] — up to 4% w/w of SO₂ or H₂SO₄ have to be added to obtain high saccharification yields [17, 20].

The main disadvantage of harsh STEX conditions is the degradation of hemicellulosic carbohydrates and the formation of secondary degradation compounds, which may inhibit microbial fermentation [17, 20, 21] and diminish overall yields of the process. To develop a pretreatment process with high carbohydrate retention and good saccharification efficiency during enzymatic hydrolysis, better understanding of the impact of pretreatment on enzyme accessibility and biomass structure is of utmost importance [15, 16].

Therefore, the aim of the present study was to analyze the impact of steam pretreatment severity on composition, ultrastructure, and enzymatic hydrolyzability of Norway spruce. To address this objective, the chemical and supramolecular properties of spruce following steam pretreatment at six different severities were determined and correlated with the enzymatic hydrolysis efficiency. A combined severity factor (CSF) summarizing the different operating parameters (temperature, residence time, and pH) into a single value [22], allows for a comparison of different pretreatment conditions. Steam pretreatment conditions were defined

by two different temperatures (180 °C and 210 °C), with/without the addition of various acids (CH₃COOH, H₃PO₄, H₂SO₄, SO₂). Overall structural properties were assessed by scanning electron microscopy (SEM). The effect of STEX severity on lignin and lignin-carbohydrate bonds was investigated by two-dimensional heteronuclear single quantum correlation nuclear magnetic resonance (2D HSQC-NMR). Finally, cellulose ultrastructure was studied by applying small/wide-angle X-ray scattering (SAXS/WAXS). The novelty of this work is the connection of different advanced structural characterization with the enzymatic hydrolyzability using six different steam pretreated spruce. The results contribute to add structural knowledge of mild steam pretreated spruce that is important to compromise between enzymes accessibility and hemicellulose retention in the solid fraction.

2 Materials and methods

2.1 Raw material and steam pretreatment

Milled Norway spruce (*Picea abies*) chips were kindly provided by the Widtskövle saw mill. Prior to pretreatment, the wood chips were reduced in size using a laboratory knife-mill (SK1; Retsch GmbH, Haan, Germany) and a 20-mm screen.

The milled spruce was pretreated by STEX then washed, pressed, and used for the hydrolysis experiment. The pretreatment was performed as previously described [18] using six different conditions as detailed in Table 1. One batch of raw material was used for pretreatment by autocatalysis and SO₂; while a second batch was used for the remaining conditions. The raw material had a DM content of 55% w/w and 2 × 750 g of material were loaded in a preheated 10-L reactor for each condition. Pretreatment with a catalyst involved an overnight pre-incubation with acid. In the case of sulfur dioxide, the raw material was incubated for 20 min with 3% (w/w) SO₂ inside a plastic bag and then exposed to air for 30 min before loading in the reactor.

After STEX, the liquid and solid fractions were separated using a hydraulic filter press at 100 bar (HP5M; Fischer Maschinenfabrik, Neuss, Germany). The solid fraction was washed using 10-L warm deionized water per kg of material, stirred for 1 h, and filter-pressed. The pretreated materials were not further processed to perform the enzymatic hydrolysis. The pH of the liquid fraction was measured to calculate the CSF for each pretreatment condition (Table 1) as detailed in Sect. 2.7.

2.2 Compositional analysis

The carbohydrate composition of raw and pretreated materials was analyzed following the National Renewable Energy Laboratory/TP-510–42,618 protocol. In the case of the raw

Table 1 Summary of the conditions applied for pretreatment of Norway spruce biomass and combined severity factor

	STEX _{180°C/aut}	STEX _{210°C/aut}	STEX _{210°C/HAc}	STEX _{210°C/H3PO4}	STEX _{210°C/H2SO4}	STEX _{210°C/SO2}
Temperature (°C)	180	210	210	210	210	210
Residence time (min)	5	5	5	5	5	5
Catalyst ^a	autocatalyzed	autocatalyzed	1% HAc	0.1% H ₃ PO ₄	0.1% H ₂ SO ₄	3% SO ₂
pH liquid fraction	3.9	3.6	3.1	2.9	2.5	1.5
CSF	0.7	1.0	1.5	1.7	2.1	3.1

^aThe percentages are expressed in w/w

HAc, acetic acid

material used for pretreatment by autocatalysis and SO₂, the analysis was performed on non-extracted material; for the raw material used for the other conditions, extracted material was used for the analysis. The difference in sample preparation of the raw material led to an overestimation of the acid insoluble lignin in the raw material not extracted (Table 2A) [49]. Monomeric sugar composition was analyzed in triplicate for each material as described in Sect. 2.7.

2.3 SEM analysis

Biomass samples were studied by SEM using a FEI Quanta 200 instrument (FEI Company, Eindhoven, The Netherlands). A small amount of material was fixed on conductive polycarbonate stickers with admixed graphite (G3347; Plano GmbH, Wetzlar, Germany) without any coating or drying

Table 2 Compositional analysis of lignocellulosic compounds in spruce before and after pretreatment. Data represent mean values ± standard deviation. Analyses were performed in triplicate. The glu-

can amount corresponds to the amount of glucose from cellulose and from galactoglucomannan

A	Raw material (%w/w DM)	STEX _{180°C/aut} (%w/w DM)	STEX _{210°C/aut} (%w/w DM)	STEX _{210°C/SO2} (%w/w DM)
Glucan	45.6 ± 0.7	49 ± 1	52 ± 2	50 ± 2
Xylan	5.0 ± 0.1	4.9 ± 0.6	2.4 ± 0.1	0.0 ± 0.0
Arabinan	0.5 ± 0.0	0.0 ± 0.0	0.0 ± 0.0	0.0 ± 0.0
Galactan	1.7 ± 0.1	1.5 ± 0.1	0.2 ± 0.0	0.0 ± 0.0
Mannan	12.1 ± 0.1	10.7 ± 0.6	4.1 ± 0.2	0.0 ± 0.0
ASL	2.6 ± 0.1	2.3 ± 0.1	1.4 ± 0.0	1.3 ± 0.0
AIL	32.4 ± 0.1	34.4 ± 0.6	41.4 ± 0.4	51.4 ± 0.5
Ash	BDL	BDL	BDL	BDL
Recovery	100 ± 1	103 ± 2	101 ± 1	103 ± 2

AIL, acid-insoluble lignin; ASL, acid-soluble lignin; BDL, below detection limit

B	Raw material (%w/w DM)	STEX _{210°C/HAc} (%w/w DM)	STEX _{210°C/H3PO4} (%w/w DM)	STEX _{210°C/H2SO4} (%w/w DM)
Glucan	45.5 ± 0.9	60.5 ± 0.3	61.3 ± 0.4	61.0 ± 0.1
Xylan	5.7 ± 0.1	1.7 ± 0.0	1.3 ± 0.0	0.7 ± 0.0
Arabinan	0.7 ± 0.3	0.0 ± 0.0	0.0 ± 0.0	0.0 ± 0.0
Galactan	1.7 ± 0.1	0.1 ± 0.0	0.1 ± 0.0	0.1 ± 0.0
Mannan	13.2 ± 0.1	1.2 ± 0.0	0.9 ± 0.0	0.6 ± 0.0
ASL	3.7 ± 0.1	2.9 ± 0.1	2.8 ± 0.1	2.7 ± 0.1
AIL	26.4 ± 0.2	36.0 ± 0.1	36.9 ± 0.1	38.2 ± 0.4
Ash	BDL	BDL	BDL	BDL
Water extractives	3.8 ± 1.5	-	-	-
Ethanol extractives	0.8 ± 0.1	-	-	-
Recovery	102 ± 3	103 ± 1	103 ± 1	103 ± 1

AIL, acid-insoluble lignin; ASL, acid-soluble lignin; BDL, below detection limit

of the material. The electron microscope was operated at an accelerating voltage of 10 kV in a low-vacuum mode.

2.4 Milled wood lignin extraction and semi-quantification of linkages

First, the pretreated material was dried at 45 °C for 48 h, milled in a laboratory SK1 knife-mill using a 0.5-mm screen, and dried for another 24 h at 45 °C. The dry coarse powder was then ball-milled for 5 days in air-tight 1-L steel containers, filled with 20 g of material and 32 stainless steel balls (10 mm in diameter), at a speed of 35 rpm. Next, 3 g of ball-milled material was weighed in extraction thimbles (26 × 60 mm; Whatman, Maidstone, England), these were transferred to 100-mL blue-cap bottles, and 50 mL of 96 wt% 1,4-dioxane (diluted from 99.8% stock; Sigma-Aldrich Co., St. Louis, MO, USA) was added. The bottle was closed and placed in an 80 °C water bath for 16 h, after which the liquid fraction was removed, another 50 mL of solvent was added, and the procedure was repeated for 16 h. The solvent from both extraction steps was combined and evaporated (Multivapor P-6; BÜCHI Labortechnik AG, Flawil, Switzerland) at 55 °C and 60 mbar overnight. The remaining MWL solid was placed in an oven at 45 °C for 48 h to fully dry.

For 2D HSQC-NMR analysis, 100 to 150 mg of dry MWL was dissolved in 600 µL deuterated DMSO- d_6 . NMR spectra were recorded at room temperature using a Bruker Avance III HD 500 MHz spectrometer (Bruker BioSpin GmbH, Karlsruhe, Germany) equipped with a 5-mm broadband probe and Z-gradient coil. The “hsqcedetgpsisp2.3” pulse program was used for HSQC at the following acquisition settings: 80 scans, 0.12 s acquisition time, 2.0 s relaxation delay, 9.5 µs pulse width, 1199 to 390 size of free induction decay, and spectral width of 19.99 and 190.20 ppm. HMBC experiments were performed with a long-range coupling constant of 6 Hz [8]. NMR spectra were processed with MestReNova 12 (Mestrelab Research S.L., Santiago de Compostela, Spain) using a 90° shifted square sine-bell apodization window, and baseline and phase correction in both dimensions. The peaks were referenced to the central DMSO peak ($\delta_C/\delta_H = 39.5/2.5$ ppm), identities were assigned according to literature [24, 27], and the unsubstituted carbon 2 of the aromatic group on lignin was used as an internal reference for semi-quantification [25].

2.5 SAXS/WAXS

SAXS and WAXS measurements were performed using Mat:Nordic from SAXSLAB (Copenhagen, Denmark). The instrument was equipped with a Rigaku 003+ high brilliance microfocus Cu radiation source (Rigaku, Tokyo, Japan) and a Pilatus 300 K detector (Dectris, Baden, Switzerland). The X-ray wavelength was 1.54 Å⁻¹, and the measured q -range was 0.007–0.25 Å⁻¹ for SAXS, 0.07–2.7 Å⁻¹ for WAXS, and

2.5–3.5 Å⁻¹ for the secondary Pilatus 100 K detector. The q -axis was calibrated using a silver behenate sample before every new set of measurements. Wet samples were sealed in sandwich cells covered with mica windows and measured at room temperature. The measurements were performed on three different spots of a sample piece. The 2D scattering patterns were radially averaged using SAXSGui software. Background subtraction and peak deconvolution for WAXS analysis was performed using Fityk software. The diffractograms were deconvoluted using Gaussian functions. In addition, cells containing Milli-Q water and soluble spruce hemicellulose (galactoglucomannan) samples extracted from spent-sulfite liquor were measured to model the amorphous peaks more accurately using two or three Gaussian functions. The diffractograms of galactoglucomannan and water are reported in the Fig. S3. The detailed chemical composition of hemicellulose samples is presented elsewhere [39]. The crystallinity index was calculated according to Eq. (11):

$$\text{Crystallinity index} = 1 - \frac{I_{\text{amorphous}}}{I_{200}} \quad (1)$$

where $I_{\text{amorphous}}$ and I_{002} are the intensity of the amorphous peak ($\sim 19^\circ$) and the 200 reflection ($\sim 22.4^\circ$) [40], respectively. The Scherrer Eq. (2) was used to estimate the apparent crystallite size (L):

$$L = \frac{K \cdot \lambda}{\beta \cdot \cos\Theta} \quad (2)$$

where K , λ , β , and Θ represent a constant of 0.94, the X-ray wavelength (1.542 Å), the half-height width of a diffraction peak, and the Bragg angle corresponding to the 200 crystalline plane, respectively. The positions of the peaks were first fixed to published values for 101 (15°), 10f (16.5°), 102 (20.4°), and 200 (22.4°) reflections and were fitted once the appropriate match was obtained. The 004 peak was not used due to poor data quality. The obtained model parameters are reported in the Table S1.

One-dimensional SAXS curves were plotted as Kratky plots (q vs. Iq^2) to enhance certain features. The maximum of the peak (q_{max}) observed in Kratky plots at around 0.11 Å⁻¹ is often used to estimate microfibril-to-microfibril distances [34, 35]. The peak maxima were determined by fitting with Gaussian functions. The dimensions (d) were then calculated using Eq. (3):

$$d = \frac{2\pi}{q_{\text{max}}} \quad (3)$$

2.6 Enzymatic hydrolysis

Two enzyme preparations, Celluclast® 1.5 L and Novozym 188 (Novozymes, Lyngby, Denmark), were used for

enzymatic hydrolysis. The enzymes were loaded based on their activity. Using the filter paper unit (FPU) assay [41] with some adjustments [42], the cellulolytic activity in Celluclast® was determined to be 50 FPU mL⁻¹. The β-glucosidase activity of Novozym 188 was determined as described previously [43]. Briefly, 50 μL of diluted enzyme solution was mixed with 50 μL of 2.0 mM *p*-nitrophenyl-β-D-glucopyranoside (in 50 mM sodium acetate buffer, pH 5.0) and incubated at 50 °C for 10 min. The reaction was stopped with 100 μL of 1 M Na₂CO₃ and the activity was determined to be 20 U mL⁻¹.

The enzymatic hydrolysis experiments were performed in triplicates, in 2-mL screw-cap tubes, and for a total reaction weight of 1.8 g. The loaded substrate (2% w/w of DM) was suspended in 0.15 M acetate buffer pH 5. The reaction mixture was autoclaved at 121 °C for 20 min, after which the sterile filtrated enzyme mixtures were added aseptically at 10 FPU g⁻¹ DM for Celluclast® 1.5 L and 10 U g⁻¹ DM for Novozym 188. The reactions were carried out at 40 °C for 48 h in an oven with a constant end-over-end rotation (Big S.H.O.T III™; Boekel Scientific, Feasterville, PA, USA) at 25 rpm. To terminate the reaction, the mixture was boiled for 10 min. The samples were then either stored at -20 °C or processed directly as detailed in Sect. 2.7.

2.7 Analytical methods and data processing

DM content was measured in triplicate as dry weight at 105 °C [44].

The release of glucose, mannose, and xylose was measured by isocratic high-performance anion-exchange chromatography with pulsed amperometric detection (ICS-5000; Dionex, Sunnyvale, CA, USA) as described elsewhere [45]. The samples were centrifuged for 5 min at 13,000 rpm, and the supernatants were filtered through 0.22 μm syringe-driven filters before storage at 4 °C until analysis.

The CSF, correlating the effects of temperature, residence time, and medium acidity with the effectiveness of biomass pretreatment [46], was calculated as explained elsewhere [47]. The conversion of polymers to soluble monomeric sugars after enzymatic hydrolysis at low solids loading was calculated by Eq. (4) [48]:

$$Y_g = \frac{C_g - C_{g0}}{\varphi_G C_{is0} X_{G0}} \quad (4)$$

where Y_g is the conversion (expressed as %) of cellulose to glucose (taken as example), C_g (g L⁻¹) is the concentration of solubilized glucose in the sample supernatant, C_{g0} (g L⁻¹) is the initial glucose concentration, φ_G is the molecular weight ratio of glucose-to-glucan monomer ($\varphi_G = 180/162 = 1.11$), C_{is0} (g L⁻¹) is the initial concentration of insoluble solids, and x_{G0} is the initial mass fraction of glucan in insoluble solids.

3 Results

3.1 Compositional characterization of mildly pretreated spruce biomass

The chemical composition of differently pretreated spruce biomass was determined. The effect of temperature and addition of acid catalysts, including acetic acid (HAc), phosphoric acid, sulfuric acid, and sulfur dioxide, was investigated using two different batches of raw material (Table 2). The CSF increased from 0.66 for STEX_{180°C/aut} to 3.1 for STEX_{210°C/SO₂}, concomitantly with a decrease in pH from 3.9 to 1.5 (Table 1).

The main difference between the pretreated materials was the extent and composition of the remaining hemicellulose (Table 2). The hemicellulose content decreased from 20% w/w DM in the raw material to 0% w/w DM in STEX_{210°C/SO₂}. Loss of arabinose on arabinoglucuronoxylan was observed in all pretreatments. Almost complete loss of galactose on galactoglucomannan occurred already with STEX_{210°C/aut}. During STEX_{210°C/HAc}, STEX_{210°C/H₃PO₄}, and STEX_{210°C/H₂SO₄}, the content of xylan and mannan decreased from 5.7 to 0.7% w/w DM and from 13.2 to 0.6% w/w DM respectively, with increasing severity. It is important to underline that the glucan amount, reported in Table 2, comprehends the amount of both glucose from cellulose and from galactoglucomannan.

4 Impact of acid-catalyzed steam pretreatment on MWL

The effect of acid-catalyzed steam pretreatment on milled wood lignin (MWL) was evaluated by 2D HSQC-NMR. MWL extraction by a modified version of the Björkman method [23] was applied to the STEX_{210°C/aut}, STEX_{210°C/HAc}, STEX_{210°C/H₃PO₄}, and STEX_{210°C/H₂SO₄}. On average, the extracted MWL amounted to 25% (w/w) of total acid-insoluble lignin, with the autocatalyzed material having the lowest yield (21% w/w) (Table 3). The reported values are within the values presented in literature which are between 10 and 25% (w/w); where the lower percentage was found for ball milled spruce and the higher for hydrothermally treated spruce [24, 25]. Generally, increasing the severity of pretreatment results in higher MWL yields [26], owing to higher mechanical or chemical interbond cleavage, which in turn increases the amount of dioxane-soluble lignin and LCCs [24]. This trend is not immediately evident from the extraction yields obtained in this study (Table 3). The apparent discrepancy could be explained by an insufficient difference in severity, leading

Table 3 Results from the extraction of MWL at varying severities. The extraction yields and the content of the inter-monomer linkages are highlighted in bold

	Acid Extraction yield (% of AIL)	STEX _{210°C/aut} 20.7	STEX _{210°C/HAc} 28.4	STEX _{210°C/H3PO4} 24.3	STEX _{210/H2SO4} 28.2
Lignin signals ^a	β-O-4	9.5	7.3	6.1	5.2
	β-5	11.9	11.4	11.1	10.0
	β-β	1.0	0.9	0.9	1.0
	Coniferyl aldehyde	5.4	3.7	4.9	3.7
	α-Carbonyl	1.6	2.0	2.8	1.9
	Methoxyl	57.5	54.7	53.4	53.8
LCC signals ^a	Gamma ester (acetyl ester)	0.7	0.6	0.7	0.6
	Gamma ester (formyl ester)	11.0	19.9	33.7	24.8
	Gamma ester (uronic acid)	5.2	5.0	5.8	4.6
	β-O-4 _{γester}	2.5	2.1	1.9	1.0
	Benzyl ether	0.1	0.1	0.2	0.3
Sugars (HPLC) ^b	Arabinan	0.4	0.3	0.4	0.3
	Galactan	0.4	0.5	0.4	0.4
	Glucan	2.5	1.4	1.5	1.2
	Xylan	0.8	0.8	0.7	0.8
	Mannan	1.3	2.5	2.4	2.1

^aFrequency per 100 aromatic rings^b(mg/g of MWL)

to only minimal structural changes between fractions, or by the extraction method reaching in a plateau.

MWL was dissolved in DMSO-*d*₆ and analyzed using 2D HSQC-NMR. As shown in Fig. 1 for the autocatalyzed fraction (STEX_{210°C/aut}), NMR signals in the aromatic region (6.1/102.0 ppm < δ_H/δ_C < 7.6/122.0 ppm) indicate that the lignin was of the guaiacyl type, with no signals for syringyl (δ_C < 102.0 ppm) and *p*-hydroxyphenyl (δ_C > 122.0 ppm), as expected for spruce lignin [27]. The major intermonomer linkages identified were β-O-4, β-5, and β-β. Methoxyl and oxidized structures (α-carbonyl and coniferyl aldehyde) were also detected (Fig. 1). While the same peaks were detected in all fractions (Fig. S2), semi-quantitative data showed differences in bond occurrence between them (Table 3). The content of β-O-4 linkages was lower than the 36–45 units/100 aromatic rings reported for ball-milled spruce lignin [25]. This discrepancy can be attributed to the harsh conditions of STEX and catalyst addition, which are known to cleave β-O-4 linkages much more effectively than ball milling [25, 28, 29]. In our study, an increase in STEX severity led to a decrement of β-O-4 linkages. A similar trend was observed for β-5 linkages, although to a lesser degree, demonstrating the stable nature of lignin carbon–carbon bonds, including β-β linkages, in acidic conditions (Table 3) [29].

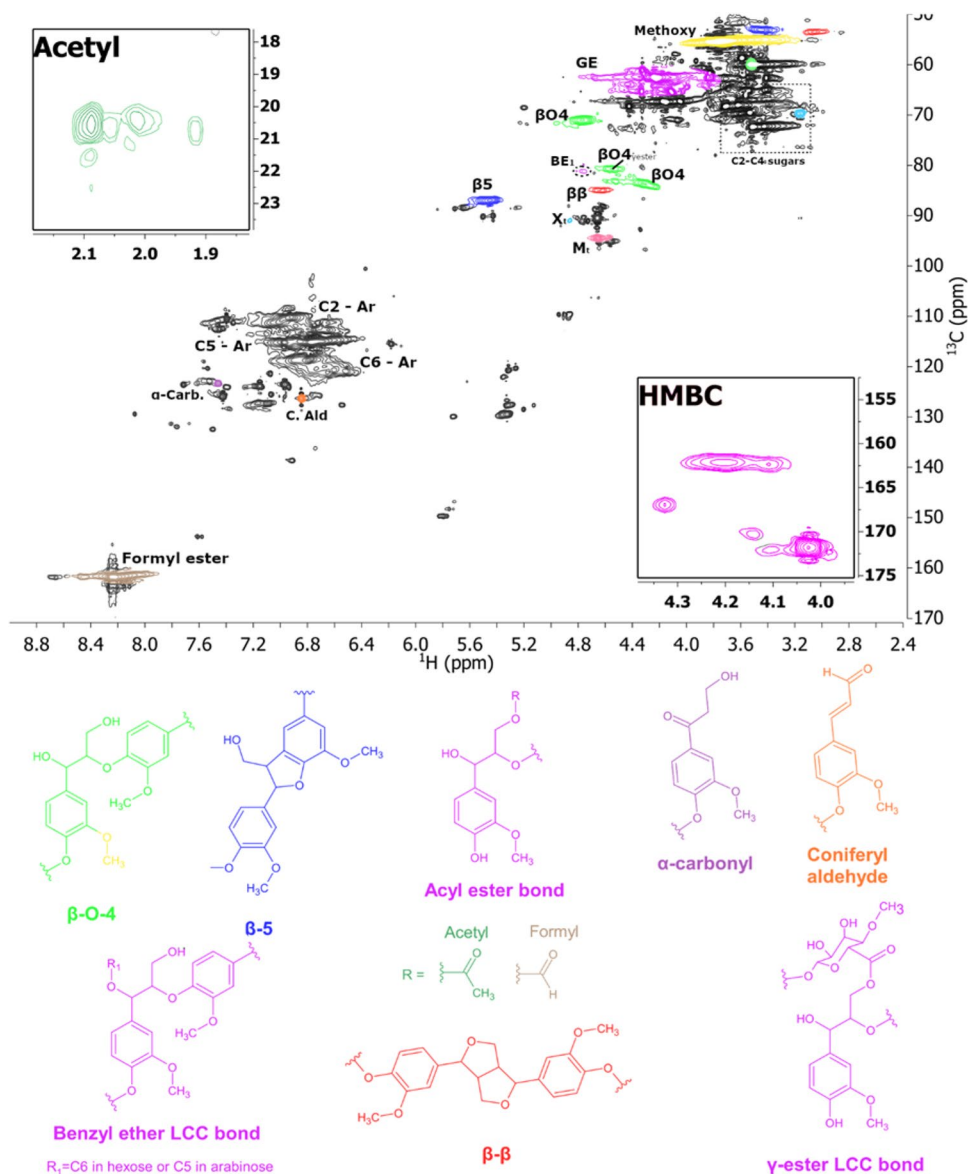
NMR spectra showed signals for two types of LCCs, gamma esters and benzyl ether (Fig. 1), implying that the sugars found in the fractions (Table 3) could be coupled to lignin through benzyl ether and gamma ester linkages. The region for gamma esters (δ_C/δ_H: 62–65/3.8–4.5 ppm) contained

several overlapping peaks due to the occurrence of two different classes of gamma ester bonds: acetyl esters (δ_C/δ_H: 62.5/4.24; 3.84 ppm) and uronic acid esterified lignins [24].

One prerequisite for the identification of acetyl esters is the presence of a methyl signal in the region for acetyl groups (δ_C/δ_H ~ 20.0/2.0 ppm) and the absence of acetylated polysaccharide signals. The latter ensures that the methyl signals originate from acetylated lignin and not from polysaccharides. These conditions were observed in Fig. 1. Giummarella and Lawoko [24] reported that these acetyl esters were part of β-O-4 subunits, which gave a signal at a chemical shift of δ_C/δ_H ~ 81/4.62 ppm, which was also observed in Fig. 1 (βO₄_{γester}). This finding strengthened the results and assignment of this gamma ester bond.

Uronic acid esterified lignins were visible in Fig. 1 (δ_C/δ_H: 65.3/4.33; 4.11 ppm). These bonds are the result of the formation of gamma-ester linkages between lignin and uronic acids [24]. The C-6 of non-esterified uronic acid produces a signal at δ_C = 171.4 ppm in a carbon NMR spectrum [8]. However, in LCC gamma ester bonds, the same signal is shifted upfield to δ_C = 166.5–169.4 ppm. The C-6 of the uronic acid group is a carbonyl carbon and not visible by HSQC. However, correlations between the C-6 of uronic acid and H-γ (³*J* long-range coupling) of lignin can be seen using heteronuclear multiple bond correlation (HMBC). Based on HMBC results (Fig. 1), a correlation was found at δ_C = 167 ppm for the signal at δ_C/δ_H: 65.3/4.33 ppm, thereby confirming that the signal was probably originating from the LCC gamma ester bond.

Fig. 1 HSQC and HMBC spectra of MWL derived from STEX_{210°C/aut}-pretreated material and dissolved in DMSO-*d*₆. The numbers in the labels indicate the carbon number in the different substructures. The identified substructures in lignin, sugars, and LCCs are shown with structure colors and labels matching the peaks in the HSQC spectra. α -Carb. = α -carbonyl; BE = benzyl ether; C. Ald = coniferyl aldehyde; C-Ar = carbon in the aromatic ring; GE = gamma ester; M = mannose; X = xylose



The HMBC results revealed an interesting correlation between the gamma ester signals at $\delta_{\text{H}} = 4.24; 4.11$ ppm and a signal at $\delta_{\text{C}} = 162$ ppm. A signal found by HSQC corresponded to the formyl ester at 162/8.22 ppm (Fig. 1). Based on the chemical shift region and assignment in literature, the signal was probably originating from a formyl group [30]. The formation of acyl groups (acetyl and formyl) is driven by Fischer's acidic esterification of carboxyl groups on acetic and formic acid with the hydroxyl groups on lignin. The concomitant presence of formyl and acetyl esters likely explains the overlapping region of gamma esters. Semi-quantitative results (Table 3) revealed different trends for the two acyl esters; the amount of acetyl esters remained largely constant at varying pretreatment severity, while the amount of formyl

ester increased with increasing severity. This trend could be related to the formation, strength, and structure of acetic and formic acids. Acetic acid is produced mainly by the hydrolysis of acetyl groups on hemicellulose, whereas formic acid is a thermochemical degradation product of polysaccharides; both of them increased with the severity of pretreatment [31]. Formic acid is stronger than acetic acid (pKa of 3.8 vs. 4.8) and is structurally more accessible due to a hydrogen on the carboxyl group versus methyl group on acetic acid. As a result, formic acid is more reactive than acetic acid [32]. As shown in Table 3, the detected gamma ester and benzyl ether bonds were stable under acidic STEX conditions, which could explain the recalcitrance of hemicellulose during steam pretreatment (Table 2) [24].

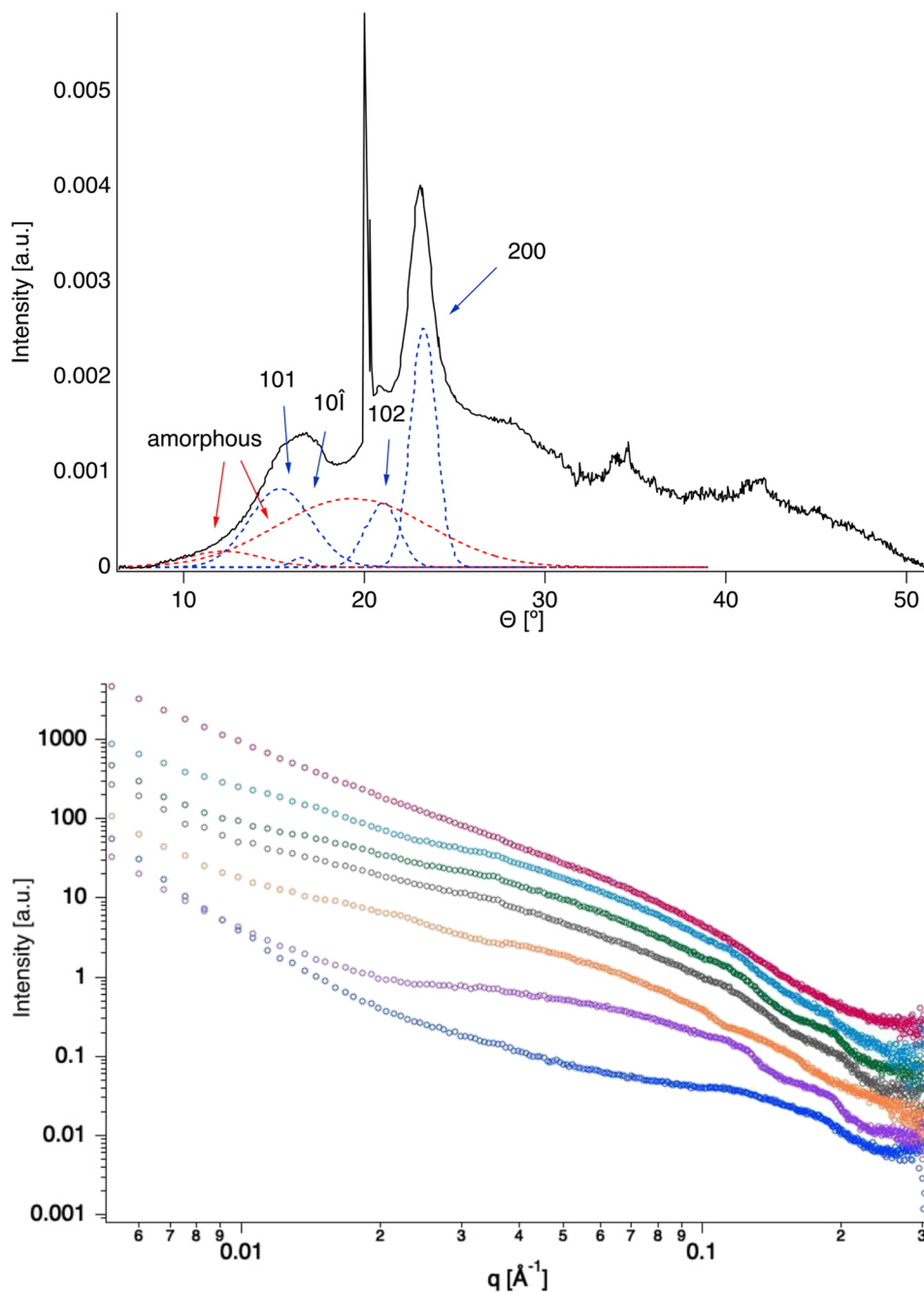
4.1 Impact of steam pretreatment severity on cellulose ultrastructure analyzed by SAXS/WAXS

The effect of lowering steam pretreatment severity on the crystallinity of cellulose microfibrils was studied by WAXS. Figure 2 showcases a typical diffractogram of a spruce sample subjected to H_2SO_4 -catalyzed STEX. The WAXS profile consisted of five characteristic crystalline peaks (101, 10 $\bar{1}$, 102, 200, and 004) and a broad amorphous region at 19°. The curve above 26° was dominated by the scattering

from water, due to the elevated moisture content in the samples. The remaining scattering curves are presented in the Fig. S2.

Once all the peaks were fitted, the crystallinity index and the size of the ordered domains were determined. Because the crystallinity index is a relative value affected by changes in both crystalline and para-crystalline parts of the cellulose structure, it is difficult to draw conclusions on the absolute content of crystalline domains. The crystallinity index of the raw material was estimated to be $63\% \pm 4\%$ (Fig. 3A) and was similar to that of autocatalyzed materials. The size of

Fig. 2 WAXS diffractogram (above) of a spruce sample treated with H_2SO_4 . Dashed lines represent theoretical fits to the experimental data. A sharp peak at around 21° corresponds to the scattering from mica windows. SAXS curves (below) of untreated spruce (dark blue) and samples pretreated by STEX_{180°C/aut} (purple), STEX_{210°C/aut} (orange), STEX_{210°C/HAc} (grey), STEX_{210°C/H3PO4} (green), STEX_{210°C/H2SO4} (light blue), and STEX_{210°C/SO2} (pink). Scattering curves were shifted for visual clarity



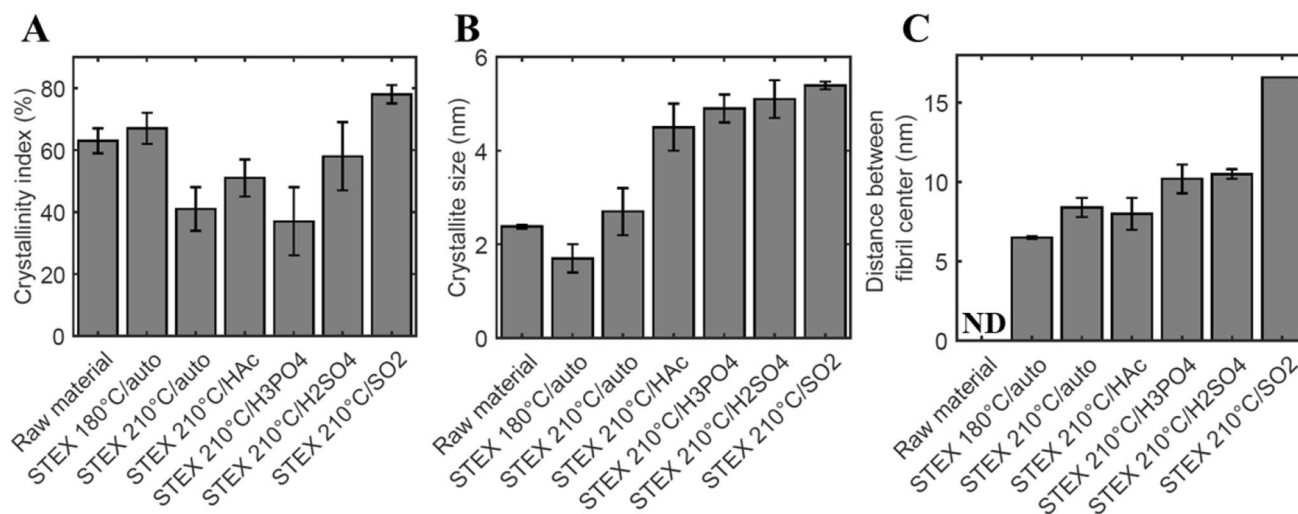


Fig. 3 Crystallinity index (A) and crystallite size (B) of raw and steam pretreated spruce samples, as determined by WAXS analysis. Distance between fibril center (C) of steam pretreated spruce sam-

ples, as determined by SAXS analysis. Error bars correspond to a standard deviation of three measurements

the cellulose crystallite in the untreated spruce sample was 2.38 ± 0.04 nm, which is comparable to 2.2 nm reported in the literature [33]. A comparison of the crystallinity index between STEX_{210°C/HAc} and STEX_{210°C/SO₂} revealed a slight increase in crystallite dimension with increasing severity of pretreatment, suggesting the aggregation of cellulose microfibrils.

SAXS provides information on the microfibril arrangement inside the plant cell wall. A typical scattering curve of wood samples often contains a characteristic peak at around 0.11 \AA^{-1} (Fig. 2). The peak was more clearly visible in a Kratky plot (Fig. S4), which included the scattering curves of spruce samples before and after pretreatment. The dimensions obtained from the center of the peak can be correlated with the microfibril-to-microfibril distance [34, 35]. The peak in the SAXS curve of the untreated spruce sample was not sufficiently pronounced, preventing any interpretation. The distance between the microfibrils' center is increasing as the pretreatments become harsher (Fig. 3C). Considering that WAXS indicated microfibrillar aggregation, we believe that the distance observed by SAXS is between cellulose microfibril aggregates instead, as the microfibrils are closely packed inside the aggregates and give rise to similar scattering.

4.2 Overall structural evaluation of mildly pretreated spruce

A macroscopic observation of the pretreated materials revealed some clear differences (Fig. S1). Compared to the raw material, the substrate presented increasingly smaller particle size and homogeneity with increasing severity of pretreatment.

SEM was used to study the effect of steam pretreatment on spruce overall structure (Fig. 4). The tracheids in softwood (Fig. 4, red arrows) are between 1 and 10 mm in length and function chiefly as a source of support (late wood) or for the conduction of fluids (early wood) [36]. The main effect of steam pretreatment was defibrillation of the wood chips' surface, which was unnoticeable in the raw material (Fig. 4A) but became increasingly evident with rising severity of pretreatment. In STEX_{180°C/autoclave}, the overall structure looked slightly corrugated (Fig. 4B), although still similar to the raw material. STEX_{210°C/autoclave} showed an increased effect on the surface (Fig. 4C), but the overall structure was akin to the material pretreated at 180 °C. The addition of acids triggered further defibrillation, and the overall structure of the material started to show disruption (Fig. 4D–F). In STEX_{210°C/SO₂}, almost complete disruption of the structure was reached because of the high severity of the pretreatment (Fig. 4G).

4.3 Evaluation of enzymatic hydrolyzability yields

To investigate the enzymatic hydrolyzability of various steam pretreated spruce samples, enzyme-catalyzed sugar release was assessed. Glucose was released from both cellulose and galactoglucomannan (Fig. 5). The release of glucose increased from 0% w/w DM in the raw material to 19% w/w DM in STEX_{210°C/H₂SO₄} and 66% w/w DM in STEX_{210°C/SO₂} (Fig. 5A). Xylose, which was released from the arabinoglucuronoxylan backbone, reached its highest value of 11% w/w DM in STEX_{210°C/autoclave} (Fig. 5B). Similarly, the largest release of mannose from the galactoglucomannan backbone (17% w/w DM) was detected in STEX_{210°C/autoclave} (Fig. 5C).

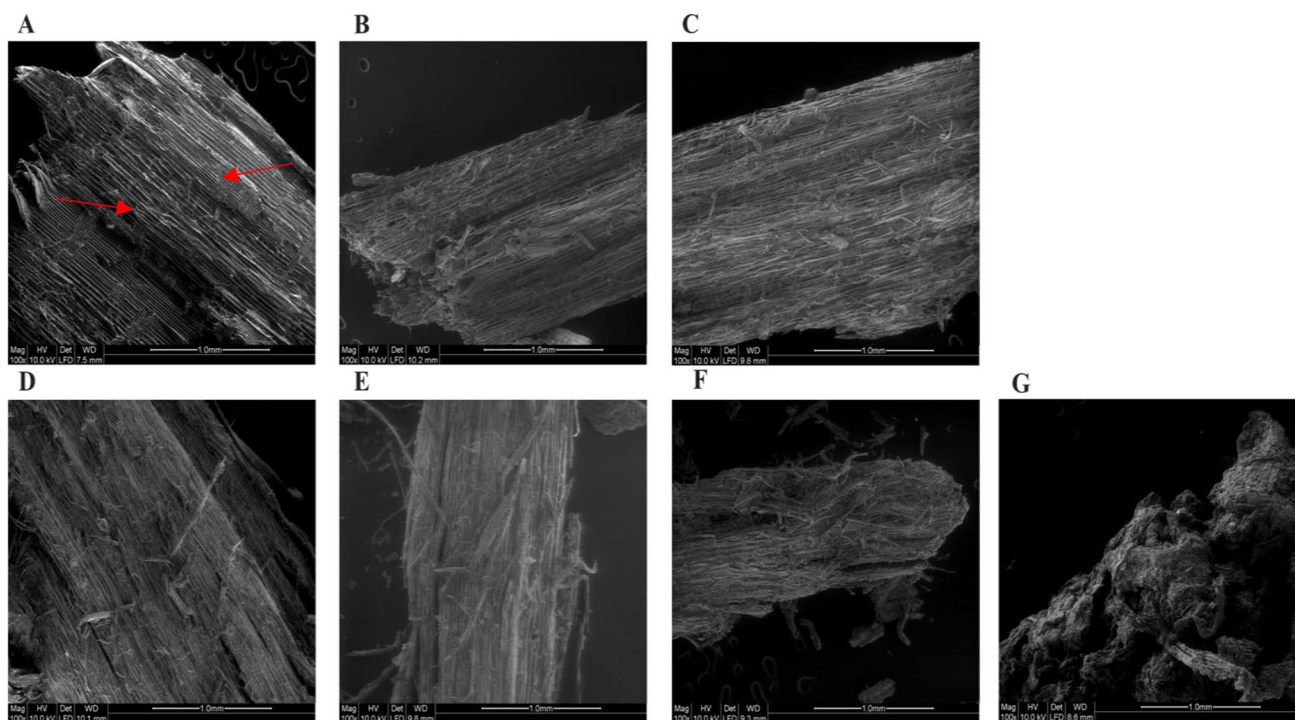


Fig. 4 SEM images showing the ultrastructure of Norway spruce before and after pretreatment. **A** Untreated sample. **B–G** Samples pretreated by **B** STEX_{180°C/auto}, **C** STEX_{210°C/auto}, **D** STEX_{210°C/HAc},

E STEX_{210°C/H₃PO₄}, **F** STEX_{210°C/H₂SO₄}, and **G** STEX_{210°C/SO₂}. The structures marked with red arrows represent tracheids. The scale bar in the lower right hand corner in all figures represent 1 mm

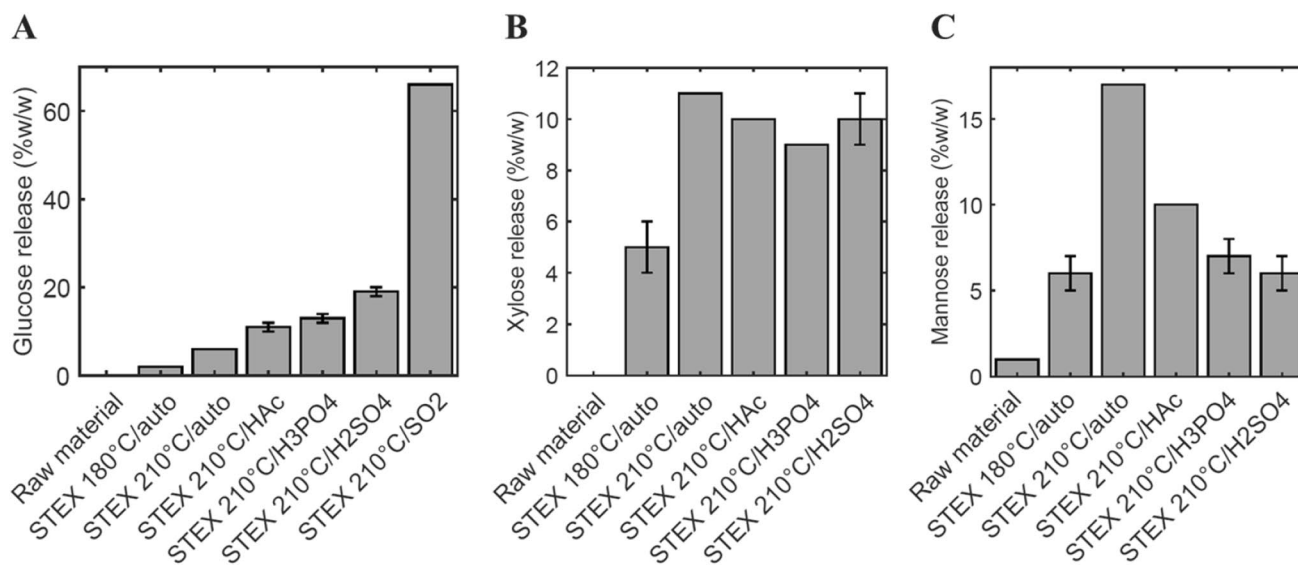


Fig. 5 Enzymatic hydrolysis of raw and pretreated spruce substrates. Release of **A** glucose, **B** xylose, and **C** mannose after 48 h of hydrolysis with an enzyme loading 10 FPUg⁻¹ DM of Celluclast and 10 U g⁻¹ DM of Novozyme 188. Yields were less accurate for materials pre-

treated at higher severities due to the small amount of residual hemicellulose in the solid fraction. Data represent mean values \pm standard deviation of triplicate measurements

5 Discussion

In the current work, spruce biomass was pretreated by STEX at different severities, and its ultrastructure was analyzed. WAXS analysis of the untreated spruce, with its even surface (Fig. 4A), was used as a starting point to understand how the cellulose crystallite size was affected by increasing pretreatment severity. The peak in the SAXS curve of the untreated spruce sample was not sufficiently pronounced, preventing any interpretation. Furthermore, no enzymatic conversion was detected. Pretreatment was essential to increase enzyme accessibility as reported frequently in the literature [5, 15, 16]. The most applied catalysts to steam pretreat softwood getting high sugars release after enzymatic hydrolysis are either sulfur dioxide or sulfuric acid [16, 17].

In the present study, sulfur dioxide was chosen as the reference catalyst because its sulfonation of lignin favors saccharification efficiencies since lignin becomes more soluble [5]. In STEX_{210°C/SO₂}, the hemicellulose was completely solubilized (Table 2A) and the overall structure was disrupted as judged by visual inspection (Fig. S1-G) and SEM (Fig. 4G). The results are in line with the expected effect of the steam pretreatment at high severities [15]. Based on the attained structural evidence, STEX_{210°C/SO₂} led to increased cellulose crystallite dimension (Fig. 3B) and the distance between the microfibrils' center (Fig. 3C), thus providing the best accessibility to enzymes, as demonstrated by the highest glucose release after enzymatic hydrolysis (Fig. 5A).

The downside of steam pretreatment with sulfur dioxide is the loss of sugars from the solid fraction and the formation of inhibitors of microbial fermentation. Both factors contribute to a decrease in the overall process yields [37]. To lower the impact on process yields, we applied milder pretreatment conditions including (from low to high severity): STEX_{180°C/aut}, STEX_{210°C/aut}, STEX_{210°C/HAc}, STEX_{210°C/H₃PO₄}, and STEX_{210°C/H₂SO₄}. The materials recovered from milder pretreatment were structurally different (Fig. 4) from STEX_{210°C/SO₂} but showed also differences between each other. Specifically, the compositional analysis revealed the loss of arabinose in all the steam pretreated materials. Almost complete loss of galactose occurred already with STEX_{210°C/aut}. During STEX_{210°C/HAc}, STEX_{210°C/H₃PO₄}, and STEX_{210°C/H₂SO₄}, the content of xylan and mannan decreased increasing the severity. Surface defibrillation and disruption of wood chips increased with increasing pretreatment severity. This effect is important for the enzymes since the presence of the fibers on the surface facilitate enzyme access. The structural observations by SEM were in line with the SAXS/WAXS and NMR results, showing rearrangement of the cellulose fibers and depolymerization of lignin.

Collectively, the results point to greater enzyme accessibility, as shown by the increase in crystallite size and the distance

between microfibrils, with rising pretreatment severity. The increase in the size of cellulose crystallites at elevated temperatures has been noted previously with different types of biomass [35, 38]. Hemicellulose acts as a spacer between microfibrils [35]; therefore, when it is removed during pretreatment, it might no longer prevent cellulose aggregation. The obtained structural information suggests that pretreatment leads to a rearrangement of cellulose microfibrils, which may cause the formation of larger pores and increase the distance between microfibril aggregates, ultimately providing easier access to enzymes [6, 12, 13]. These differences in the cellulose structure were supported by hydrolyzability results (Fig. 5A) since the glucose release increased increasing the severity of the pretreatment.

A comparison of the lignin recovered from STEX_{210°C/aut}, STEX_{210°C/HAc}, STEX_{210°C/H₃PO₄}, and STEX_{210°C/H₂SO₄} pretreatments revealed a progressive loss of β-O-4 linkages. A similar trend but less pronounced was observed in β-5 linkages that confirmed the stable nature of lignin carbon-carbon bonds in acidic conditions (Table 3) [29]. NMR spectra revealed the presence of two different signals for LCCs: gamma esters and benzyl ether. We were not able to distinguish the single gamma ester signals because of partial peak overlap between acetyl esters and uronic acid esterified lignins.

Results from MWL extraction (Table 3) showed the presence of monomeric sugars that were not solubilized during samples preparation. This is probably indicative of recalcitrance of some polymers and is in line with the evaluation of hemicellulose hydrolyzability. The release of xylose during enzymatic hydrolysis (Fig. 5B) did not increase markedly with the severity of pretreatment; whereas that of mannose decreased (Fig. 5C) increasing the severity in the materials pretreated with acids. This finding may be explained by the low amount of hemicellulose, together with that the hemicellulose may be hard to access for the enzymes because of the presence of LCCs.

6 Conclusions

The material and energy-efficient use of lignocellulosic biomass is an important priority in maximizing the overall yield of biorefinery processes. By modulating the severity of pretreatment, the use of all parts of biomass and the enzyme accessibility can be improved. By applying advanced characterization methods, novel structural knowledge on the effects of mild steam pretreatment was generated. We investigated six different pretreatment conditions and found that lowering the severity of steam pretreatment had a differential impact on the overall structure, cellulose ultrastructure, and lignin-lignin bonds of Norway spruce. Surface defibrillation and

lignin depolymerization were observed increasing pretreatment severity. Further, lignin-carbohydrate complexes signals were detected. Cellulose analysis revealed the rearrangement of microfibrils leading to the formation of larger microfibril aggregates during the pretreatment. This microfibril rearrangement likely contributed to the observed increase in enzymatic hydrolysis yields as better enzyme accessibility resulted. The added knowledge is important to understand the structural characteristics of mild steam pretreated spruce that can drive the enzyme choice for an efficient saccharification process. An efficient saccharification yield, is a prerequisite for high overall yields of the process.

Abbreviations *SEM*: Scanning electron microscopy; *STEX*: Steam pretreatment; *2D-HSQC-NMR*: Two-dimensional heteronuclear single quantum correlation nuclear magnetic resonance; *WAXS*: Wide-angle X-ray scattering; *SAXS*: Small-angle X-ray scattering; *DM*: Dry mass; *LCCs*: Lignin-carbohydrate complexes; *CSF*: Combined severity factor; *HAc*: Acetic acid; *MWL*: Milled wood lignin; *HMBC*: Heteronuclear multiple bond correlation; *FPU*: Filter paper unit

Supplementary Information The online version contains supplementary material available at <https://doi.org/10.1007/s13399-022-03405-0>.

Acknowledgements The project was supported by the Swedish Energy Agency (grant nr. 2019-021473) and LO, VN, and PN acknowledge support from Wallenberg Wood Science Center. The Chalmers Material Analysis Laboratory is gratefully acknowledged for providing experimental resources.

Author contribution FC, BA, OW, and LO conceptualized and designed the study. FC, BA, PN, and VN performed the experiments, and all authors contributed to data interpretation. FC, BA, PN, LO, and VN wrote the manuscript. All authors read and approved the final manuscript.

Funding Open access funding provided by Chalmers University of Technology.

Data availability All data generated or analyzed during this study are included in this published article and its supplementary files.

Declarations

Ethics approval and consent to participate Not applicable.

Consent for publication Not applicable.

Competing interests The authors declare no competing interests.

Open Access This article is licensed under a Creative Commons Attribution 4.0 International License, which permits use, sharing, adaptation, distribution and reproduction in any medium or format, as long as you give appropriate credit to the original author(s) and the source, provide a link to the Creative Commons licence, and indicate if changes were made. The images or other third party material in this article are included in the article's Creative Commons licence, unless indicated otherwise in a credit line to the material. If material is not included in the article's Creative Commons licence and your intended use is not permitted by statutory regulation or exceeds the permitted use, you will need to obtain permission directly from the copyright holder. To view a copy of this licence, visit <http://creativecommons.org/licenses/by/4.0/>.

References

1. Leong HY, Chang CK, Khoo KS, Chew KW, Chia SR, Lim JW et al (2021) Waste biorefinery towards a sustainable circular bioeconomy: a solution to global issues. *Biotechnol Biofuels* 14(1):1–15. <https://doi.org/10.1186/s13068-021-01939-5>
2. Mutturi S, Palmqvist B, Lidén G (2014) Developments in bioethanol fuel-focused biorefineries. *Adv Biorefineries Biomass Waste Supply Chain Exploit* 1:259–302
3. Várnai A, Siika-aho M, Viikari L (2010) Restriction of the enzymatic hydrolysis of steam-pretreated spruce by lignin and hemicellulose. *Enzyme Microb Technol* 46(3–4):185–193
4. Terrett OM, Dupree P (2019) Covalent interactions between lignin and hemicelluloses in plant secondary cell walls. *Curr Opin Biotechnol* 56:97–104. <https://doi.org/10.1016/j.copbio.2018.10.010>
5. Leu SY, Zhu JY (2013) Substrate-related factors affecting enzymatic saccharification of lignocelluloses: our recent understanding. *Bioenerg Res* 6:405–415
6. Wang Z, Winstrand S, Gillgren T, Jönsson LJ (2018) Chemical and structural factors influencing enzymatic saccharification of wood from aspen, birch and spruce. *Biomass Bioenerg* 109(February):125–134
7. Scheller HV, Ulvskov P (2010) Hemicelluloses. *Annu Rev Plant Biol* 61:263–89. <https://doi.org/10.1146/annurev-arplant-042809-112315>
8. Balakshin MY, Capanema EA, Chang HM (2007) MWL fractionation with a high concentration of lignin-carbohydrate linkages: isolation and 2D NMR spectroscopic analysis. *Holzforschung* 61(1):1–7. <https://doi.org/10.1515/HF.2007.001/html>
9. Giummarella N, Pu Y, Ragauskas AJ, Lawoko M. (2019) A critical review on the analysis of lignin carbohydrate bonds. *Green Chem* 21(7):1573–95. Available from: <https://doi.org/10.1039/c8gc03606c>
10. Koshijima T and Watanabe T (2004) Review: association between lignin and carbohydrates in wood and other plant tissues 77:175–176
11. Meng X, Ragauskas AJ (2014) Recent advances in understanding the role of cellulose accessibility in enzymatic hydrolysis of lignocellulosic substrates. *Curr Opin Biotechnol* 27:150–158. <https://doi.org/10.1148/ryct.2020200075>
12. Novy V, Nielsen F, Olsson J, Aïssa K, Saddler JN, Wallberg O, Galbe M (2020) Elucidation of changes in cellulose ultrastructure and accessibility in hardwood fractionation processes with carbohydrate binding modules. *ACS Sustainable Chem Eng* 8:6767–6776. Available from: <https://doi.org/10.1021/acsschemeng.9b07589>
13. Peciulyte A, Karlström K, Larsson PT, Olsson L (2015) Impact of the supramolecular structure of cellulose on the efficiency of enzymatic hydrolysis. *Biotechnol Biofuels* 8(1):1–13
14. Novy V, Aïssa K, Nielsen F, Straus SK, Ciesielski P, Hunt CG et al (2019) Quantifying cellulose accessibility during enzyme-mediated deconstruction using 2 fluorescence-tagged carbohydrate-binding modules. *Proc Natl Acad Sci U S A* 116(45):22545–22551
15. Galbe M, Wallberg O (2019) Pretreatment for biorefineries : a review of common methods for efficient utilisation of lignocellulosic materials. *Biotechnol Biofuels* 1–26:294. Available from: <https://doi.org/10.1186/s13068-019-1634-1>
16. Galbe M, Zacchi G 2012 Pretreatment: The key to efficient utilization of lignocellulosic materials. *Biomass and Bioenergy*. 46:70–78. Available from: <https://doi.org/10.1016/j.biombioe.2012.03.026>
17. Pielhop T, Amgarten J, Von Rohr PR, Studer MH (2016) Steam explosion pretreatment of softwood: the effect of the explosive decompression on enzymatic digestibility. *Biotechnol Biofuels* 9(1):1–13

18. Pereira Ramos L (2003) The chemistry involved in the steam treatment of lignocellulosic materials. *Quim Nova* 26(6):863–71. <https://doi.org/10.1590/S0100-40422003000600015>
19. Al-Rudainy B (2020) Galactoglucomannan recovery from softwood spent sulfite liquor challenges, process design and techno-economic evaluations. Lund university, Chemical engineering
20. Wang Z, Wu G, Jönsson LJ (2018) Effects of impregnation of softwood with sulfuric acid and sulfur dioxide on chemical and physical characteristics, enzymatic digestibility, and fermentability. *Bioresour Technol* 247(2017):200–208. Available from: <https://doi.org/10.1016/j.biortech.2017.09.081>
21. Sjulander N, Kikas T (2020) Origin, impact and control of lignocellulosic inhibitors in bioethanol production—A review. *Energies* 13:4751. <https://doi.org/10.3390/en13184751>
22. Kim Y, Kreke T, Mosier NS, Ladisch MR (2014) Severity factor coefficients for subcritical liquid hot water pretreatment of hardwood chips. *Biotechnol Bioeng* 111(2):254–263
23. Björkman A (1956) Studies on finely divided wood. Part I. Extraction of lignin with natural solvents. *Svensk Papperstidn* 59:477–485
24. Giummarella N, Lawoko M (2017) Structural insights on recalcitrance during hydrothermal hemicellulose extraction from wood. *ACS Sustainable Chem Eng*. <https://doi.org/10.1021/acssuschemeng.7b00511>
25. Giummarella N, Zhang L, Henriksson G, Lawoko M (2016) Structural features of mildly fractionated lignin carbohydrate complexes (LCC) from spruce †. *RSC Adv* 6:42120. <https://doi.org/10.1039/c6ra02399a>
26. Capanema E, Balakshin M, Katahira R, Hou-min C and Hasan J (2015) How well do MWL and CEL preparations represent the whole hardwood lignin? *J Wood Chem Technol* 35(1):17–26. <https://doi.org/10.1080/02773813.2014.892993>
27. Wallberg O, Al-Rudainy B, Galbe M, Schagerlöf H (2018) Antisolvent precipitation of hemicelluloses, lignosulfonates and their complexes from ultrafiltered spent sulfite liquor (SSL). *Holzforchung* 72(10):839–850
28. Shao S, Zhenfu AE, Guifeng JA, Ae W, Iiyama K, Shao S et al (2009) Thermo characteristics of steam-exploded bamboo (*Phyllostachys pubescens*) lignin. *Wood Sci Technol* 43:643–652
29. Yang H, Li J, Xu J, Mo L (2017) The critical analysis of catalytic steam explosion pretreatment of corn stalk, lignin degradation, recovery, and characteristic variations. *BioResources* 12(1):344–361
30. Ma Q, Li Z, Guo L, Zhai H, Ren H (2021) Formation of high carbohydrate and acylation condensed lignin from formic acid-acetic acid-H₂O biorefinery of corn stalk rind. *Ind Crops Prod* 1(161):113165
31. Jönsson LJ, Alriksson B, Nilvebrant NO (2013) Bioconversion of lignocellulose: inhibitors and detoxification. *Biotechnol Biofuels* 6:16. <https://doi.org/10.1186/1754-6834-6-16>
32. Cha JS, Um BH (2020) Delignification of pinecone and extraction of formic acid in the hydrolysate produced by alkaline fractionation. *Appl Biochem Biotechnol* 192(1):103–119. <https://doi.org/10.1007/s12010-020-03311-z>
33. Jakob HF, Fengel D, Tschegg SE, Fratzl P (1995) The elementary cellulose fibril in *Picea abies*/ comparison of transmission electron microscopy, small angle x-ray scattering and wide angle x-ray scattering results. *Macromolecules* 28:8782–8787
34. Virtanen T, Penttilä PA, Maloney TC, Grönqvist S, Kampuri T, Vehviläinen M et al (2015) Impact of mechanical and enzymatic pretreatments on softwood pulp fiber wall structure studied with NMR spectroscopy and X-ray scattering. *Cellulose* 22(3):1565–1576
35. Brännvall E, Larsson PT, Stevanic JS (2021) Changes in the cellulose fiber wall supramolecular structure during the initial stages of chemical treatments of wood evaluated by NMR and X-ray scattering. *Cellulose* 28(7):3951–3965
36. Wiedenhoef A (2014) Structure and Function of Wood: Wood Handbook. Chapter 3, Forest Products Library. General Technical report FPL–GTR–190. http://www.fpl.fs.fed.us/documnts/fplgtr/fplgtr190/chapter_03.pdf.htm
37. Novy V, Longus K, Nidetzky B (2015) From wheat straw to bioethanol: integrative analysis of a separate hydrolysis and co-fermentation process with implemented enzyme production. *Biotechnol Biofuels* 8(1):1–12
38. Xu F, Shi YC, Wang D (2012) Structural features and changes of lignocellulosic biomass during thermochemical pretreatments: a synchrotron X-ray scattering study on photoperiod-sensitive sorghum. *Carbohydr Polym* 88(4):1149–1156. Available from: <http://dx.doi.org/https://doi.org/10.1016/j.carbpol.2012.01.041>
39. Naidjonoka P, Fornasier M, Pålsson D, Rudolph G, Al-Rudainy B, Murgia S et al. (2021) Bicontinuous cubic liquid crystalline phase nanoparticles stabilized by softwood hemicellulose. *Colloids Surfaces B Biointerfaces* 203:111753. Available from: <https://doi.org/10.1016/j.colsurfb.2021.111753>
40. Popescu CM, Dobele G, Rossinskaja G, Dizhbite T, Vasile C (2007) Degradation of lime wood painting supports. Evaluation of changes in the structure of aged lime wood by different physico-chemical methods. *J Anal Appl Pyrolysis* 79(1–2):71–7
41. Ghose TK (1987) Measurements of cellulase activities. *Pure Appl Chem* 59(2):257–268
42. Novy V, Nielsen F, Cullen D, Sabat G, Houtman CJ, Hunt CG (2021) The characteristics of insoluble softwood substrates affect fungal morphology, secretome composition, and hydrolytic efficiency of enzymes produced by *Trichoderma reesei*. *Biotechnol Biofuels* 14(1):1–17. Available from: <https://doi.org/10.1186/s13068-021-01955-5>
43. Takashima S, Nakamura A, Hidaka M, Masaki H, Uozumi T (1999) Molecular cloning and expression of the novel fungal -glucosidase genes from *Humicola grisea* and *Trichoderma reesei*. *J Biochem* 125(4):728–36. Available from: <https://academic.oup.com/jb/article-lookup/doi/https://doi.org/10.1093/oxfordjournals.jbchem.a022343>
44. Sluiter A, Hames B, Hyman D, Payne C, Ruiz R, Scarlata C et al (2008) Determination of total solids in biomass and total dissolved solids in liquid process samples biomass and total dissolved solids in liquid process samples. Technical Report NREL/TP-510 42621. http://www.nrel.gov/biomass/analytical_procedures.html
45. Arnling Bååth J, Mazurkewich S, Knudsen RM, Poulsen JCN, Olsson L, Lo Leggio L et al. (2018) Biochemical and structural features of diverse bacterial glucuronoyl esterases facilitating recalcitrant biomass conversion. *Biotechnol Biofuels* 11(1):1–14. Available from: <https://doi.org/10.1186/s13068-018-1213-x>
46. Kellock M, Maaheimo H, Marjamaa K, Rahikainen J, Zhang H, Holopainen-Mantila U et al (2019) Effect of hydrothermal pretreatment severity on lignin inhibition in enzymatic hydrolysis. *Bioresour Technol* 280:303–312
47. Chum HL, Johnson DK, Black SK, Overend RP (1990) Pretreatment-catalyst effects and the combined severity parameter. *Appl Biochem Biotechnol* 24(1):1–14. Available from: <https://link.springer.com/article/https://doi.org/10.1007/BF02920229>
48. Zhu Y, Malten M, Torry-Smith M, McMillan JD, Stickel JJ (2011) Calculating sugar yields in high solids hydrolysis of biomass. *Bioresour Technol* [Internet] 102(3):2897–903. Available from: <http://dx.doi.org/https://doi.org/10.1016/j.biortech.2010.10.134>
49. Sannigrahi P, Kim DH, Jung S, Ragauskas A (2011) Pseudo-lignin and pretreatment chemistry. *Energy Environ Sci* 4(4):1306–10. <https://doi.org/10.1039/c0ee00378f>

Publisher's note Springer Nature remains neutral with regard to jurisdictional claims in published maps and institutional affiliations.